Mesoscale hydrodynamics via stochastic rotation dynamics: Comparison with Lennard-Jones fluid

Matt K. Petersen,[1,2,a)] Jeremy B. Lechman,[2] Steven J. Plimpton,[2] Gary S. Grest,[2] Pieter J. in 't Veld,[2,3] and P. R. Schunk[2]
[1]*Department of Chemistry and Center for Biophysical Modeling and Simulation, University of Utah, Salt Lake City, Utah 84112-0850, USA*
[2]*Sandia National Laboratories, Albuquerque, New Mexico 87185, USA*
[3]*Polymer Research, BASF SE, 67056 Ludwigshafen, Germany*

(Received 4 August 2009; accepted 8 April 2010; published online 6 May 2010)

Stochastic rotation dynamics (SRD) is a relatively recent technique, closely related to lattice Boltzmann, for capturing hydrodynamic fluid flow at the mesoscale. The SRD method is based on simple constituent fluid particle interactions and dynamics. Here we parametrize the SRD fluid to provide a one to one match in the shear viscosity of a Lennard-Jones fluid and present viscosity measurements for a range of such parameters. We demonstrate how to apply the Müller-Plathe reverse perturbation method for determining the shear viscosity of the SRD fluid and discuss how finite system size and momentum exchange rates effect the measured viscosity. The implementation and performance of SRD in a parallel molecular dynamics code is also described. © *2010 American Institute of Physics*. [doi:10.1063/1.3419070]

I. INTRODUCTION

Recent interest in nanoscale modeling and simulation of complex fluids led to advances in a number of mesoscale techniques. These techniques are particularly applicable for modeling suspensions in which there are large particles suspended in a background solvent. Because of the disparity in size between the particles and solvent, there can be a clear separation of time and length scales in the motion of the solvent and that of the particles. This allows one to coarse grain the solvent, making simulations of colloidal suspensions tractable. However, in so doing one must be careful not to ignore long range hydrodynamic interactions such as in simple Brownian dynamics methods. One way to include hydrodynamic interactions is to assume that the solvent can be modeled by the traditional Navier–Stokes equations, which can be then solved by finite element techniques. However this approach ignores relevant nanoscale phenomena in the fluid such as thermal fluctuations and the discrete nature of the solvent, which can become particularly important when the particles are not much larger than the solvent, as in the case of nanoparticle suspensions. Techniques that capture hydrodynamic effects at a scale somewhere between the full atomistic detail and the macroscale of the Navier–Stokes equations provide a valuable tool for modeling a range of interesting systems. While some have sought to bridge this gap by combining Brownian dynamics with Stokesian dynamics,[1] or adding Brownian-type dynamics to lattice-Boltzmann methods,[2] others have developed techniques that seek to directly coarse-grain the solvent dynamics to account for mesoscale behavior, e.g. dissipative particle dynamics (DPD).[3]

A relatively recent technique, closely related to Lattice Boltzmann, for capturing hydrodynamics at the mesoscale is stochastic rotation dynamics (SRD).[4] This technique is based on simple fluid-particle interactions and dynamics. The fluid particles are considered massive, ideal, point particles which do not interact with each other in a pairwise sense, but which interact with nanoparticles through a "coarse-grained" collision operator in such a way as to conserve energy and momentum and produce fluctuating hydrodynamic behavior. This method has been used to model colloidal suspensions,[5,6] including clustering and sedimentation[7–12] and shear flow.[13–16] Since the SRD particles are ideal point particles, unphysical depletion forces can be controlled[11] compared to those introduced when modeling colloidal suspensions as occurring with DPD and related models where the coarse grained solvent occupies a large excluded volume. For a recent review of the SRD method see Gompper *et al.*[17] and Kapral.[18]

While others investigated the transport coefficients for SRD to verify theoretical predictions,[19–25] little effort has been made to map an SRD fluid to a "real" solvent. In addition, in many previous SRD simulations with suspended particles, there has been a "telescoping" of time scales.[9,11,17] This is possible due to the wide spread in time scales between the fluid and the particles. Thus the simulated system is only "dynamically similar" to the physical system in the sense that key dimensionless numbers (e.g., Peclet, Reynolds, Schmidt, Knudsen Numbers, etc.) are kept equivalent or within an "appropriate" range. However for modeling the flow of a pure fluid or when the suspended particles are comparable in size to that of the solvent, for example in the case of nanoparticles or for a polymer whose monomers are on the same size as that of the solvent, one can map the shear viscosity of the SRD fluid to that of real fluids. It is possible to avoid the "telescoping" of time scales and chose SRD parameters so that the shear viscosity η of the SRD fluid is

a)Electronic mail: matt@hac.utah.edu.

exactly equal to that of the solvent. In this way one can evaluate the SRD method directly as a numerical technique for solving the equations of fluctuating hydrodynamics. Here we achieve both of these conditions by parametrizing the SRD fluid relative to a pure Lennard-Jones (LJ) fluid. Similar mappings can be achieved for other solvents such as water. We focus on η because it is the viscosity of the solvent that is the relevant parameter for colloidal suspension transport, e.g., η sets the scale for colloidal diffusion as can be seen from the Stokes–Einstein relation for the diffusion constant $D=k_BT/(6\pi\eta R)$ in the dilute limit, where R is the radius of the colloidal particle.

To measure the shear viscosity of the SRD fluid we employed the Müller-Plathe (MP) reverse perturbation method.[26] The MP method induces a shear profile in the fluid through an exchange of particle momentum. The shear viscosity is related to this velocity gradient through the imposed momentum transfer. Since the momentum flux is known, the viscosity is found by simply measuring the induced velocity profile. The MP method is straightforward to implement and has the added advantage of conserving both energy and linear momentum, alleviating the need for thermostating. The MP method has been applied to measure the shear viscosity of simple fluids,[26] diblock copolymers,[27] nanoparticle suspensions,[28] and ionic liquids,[29] though it has not been applied to SRD fluids. Given the unique properties of the SRD fluid—nonuniform momentum flux within an SRD bin for example—use of the MP method with an SRD fluid requires special consideration, which we discuss.

In the next section we review briefly the basics of the SRD method. We also describe the implementation of the MP reverse perturbation method for an SRD fluid. In Sec. III, we discuss how to choose SRD parameters so that the SRD properties match those of a LJ fluid and present results for the viscosity for five sets of SRD parameters. The effect of varying the MP exchange rate and particle velocity on the momentum and resulting viscosity within the SRD method are investigated. Finite size effects on the viscosity are also discussed. In Sec. IV, we describe a parallel implementation of SRD and compare its computational requirements to a LJ fluid.

II. STOCHASTIC ROTATION DYNAMICS: METHODS AND IMPLEMENTATION

SRD (Ref. 4) is a member of a class of techniques referred to as multiparticle collision dynamics,[17] which are off-lattice, particle-based simulation techniques that attempt to efficiently resolve important "mesoscale" phenomena, such as fluctuating hydrodynamics (mass and momentum conservation) at the cost of losing detailed microscopic information. The SRD algorithm consists of two steps: (i) particle streaming and (ii) particle velocity update. These are described in the following subsection. Additionally, a method for shearing SRD solvents is described.

A. The basic algorithm: Equilibrium

Consider a system of ideal, point particles of mass m_{SRD} which are sorted into bins arranged in a regular cubic lattice of size Δx. Initially, the simulation domain is seeded with these particles at uniformly random locations $\mathbf{r}_i$ and with velocities $\mathbf{v}_i$ also drawn from a uniform distribution between $[-\mathbf{v}_{\max},\mathbf{v}_{\max}]$. Since SRD is a microcononical-type method the total initial kinetic energy will determine the temperature, k_BT (i.e., the width of the Maxwell distribution, $\sqrt{k_BT/m_{\mathrm{SRD}}}$) after relaxation to equilibrium. Alternatively, one can draw the initial velocities from a Maxwell distribution with the desired temperature.

SRD involves alternating particle streaming and velocity update steps. During the streaming step, the ith SRD particle's position at time $n+1$ is calculated via the simple forward Euler scheme

$$\mathbf{r}_i^{n+1} = \mathbf{r}_i^n + \mathbf{v}_i^n \Delta t, \tag{1}$$

where Δt is the SRD time step. Following this advection of particle positions the velocity update is performed. SRD gets its name from the multiparticle collisional model embodied by the rotation matrix $\mathbf{R}[\zeta(\mathbf{r}_i^{n+1})]$ in the velocity update Eq. (2).

$$\mathbf{v}_i^{n+1} = \mathbf{v}_i^n + \mathbf{R}[\zeta(\mathbf{r}_i^{n+1})]\{\mathbf{v}_i^n - \mathbf{u}[\zeta(\mathbf{r}_i^{n+1})]\}, \tag{2}$$

where $\mathbf{u}(\zeta,t)=\Sigma_{k\in\zeta}\mathbf{v}_k/N_{\zeta,t}$ is the average velocity of bin ζ, and $N_{\zeta,t}$ is the total number of SRD particles in the bin at time t. All particles i located in bin $\zeta(\mathbf{r}_i^{n+1})$ at time level $n+1$ have the fluctuating part of their velocities rotated about a randomly chosen direction an amount $\pm\alpha$ with probability 1/2. In the current implementation, the value of α is set to $\alpha=\pi/2$; although a larger value can be beneficial.[30] In addition, here the random directions are specified to be one of the three coordinate axes chosen with probability 1/3. This information is contained in the set of matrices $\mathbf{R}$ to be drawn from.

At equilibrium the SRD particles have a Maxwell velocity distribution from which the mean free path can be determined

$$\lambda = \Delta t\sqrt{k_BT/m_{\mathrm{SRD}}}. \tag{3}$$

It is known that $\lambda \leq \Delta x/2$ results in significant loss of Galilean invariance. This can be corrected by a slight modification to the algorithm which involves a random shift of the SRD bins before the velocity update step and then shifting the bins back.[19,31] We also implemented this algorithm and tested our results both with and without the random shift. For the mapping to Lennard-Jones fluids as studied here the majority of results are for parameter sets which satisfy $\lambda \geq \Delta x/2$. Additional upper bounds on λ may be imposed by other length scales in the problem (e.g., the size of suspended colloids) as well as by practical considerations such as the size of the ghost region used for interprocessor communications. Also, it should be noted that the form of the algorithm discussed here does not conserve angular momentum. While this is not relevant for the cases considered here it is relevant for certain applications. The algorithm can be modified, but at additional computational cost.[17]

B. SRD model parameters

For a reference system we chose a standard Lennard-Jones fluid since it is the most widely modeled fluid system. The interaction between particles of mass m_{LJ} is given by

$$U_{LJ}(r) = \begin{cases} 4\epsilon\left[\left(\frac{\sigma}{r}\right)^{12} - \left(\frac{\sigma}{r}\right)^{6}\right] & \text{for } r < r_c \\ 0 & \text{for } r \geq r_c \end{cases}, \quad (4)$$

where ϵ and σ are the units of energy and distance. We carried out molecular dynamics simulations for 2592 particles at temperature at $T=1.0\epsilon/k_B$ and pressure $P=0$ for $r_c=3.0\sigma$. The resulting density $\rho=0.66m_{\mathrm{LJ}}/\sigma^3$ and kinetic viscosity $\nu=1.53\pm0.05\sigma^2/\tau$, where $\tau=\sigma(m_{\mathrm{LJ}}/\epsilon)^{1/2}$.

Accordingly, transport coefficients have been worked out for various SRD schemes using a range of approaches.[19–25] For the current implementation of rotation around orthogonal axes by a fixed amount $\pm\pi/2$, the kinetic viscosity $\nu=\eta/\rho$, where ρ is the solvent density, as derived from Green–Kubo relations[21,22] is

$$\nu = \frac{\Delta x^2}{18\Delta t}\left(1 - \frac{1-\exp(-M)}{M}\right) + \frac{k_B T \Delta t}{4\rho\Delta x^3}\left(\frac{M(M+2)}{M-1}\right), \quad (5)$$

where M is the average number of SRD particles per bin and $\rho=Mm_{\mathrm{SRD}}/\Delta x^3$ is the SRD fluid density.

In addition, for $\alpha=\pi/2$, the self-diffusion coefficient (ignoring enhancement of this transport coefficient due to correlations in the small mean free path limit)[32] can be found as follows:

$$D_f = \frac{Mk_B T\Delta t}{2\rho\Delta x^3}\left(\frac{3M}{M-1+e^{-M}} - 1\right). \quad (6)$$

Taking the ratio of these two gives an expression for the Schmidt number (see Ref. 30).

$$\mathrm{Sc} = \frac{\nu}{D_f} = \left(\frac{\Delta x}{\lambda}\right)^2 \frac{(M-1+e^{-M})^2}{M(2M+1-e^{-M})} + \frac{1}{2}\left(\frac{M+2}{M-1}\right)\frac{M-1+e^{-M}}{2M+1-e^{-M}}. \quad (7)$$

For pure fluids Sc is significant in that it indicates the relative importance of momentum and mass transport. Significant differences in the dynamics of the SRD fluid can exist depending on its value.[30] For typical liquids $\mathrm{Sc}\sim10^2$ or higher, while for the LJ liquid in view here $\mathrm{Sc}\sim10$.[33]

Equations (3) and (5) are used to determine the SRD computational parameters. Given values for k_BT and fluid material parameters ν and ρ, an equation relating the SRD fluid parameters can be found by solving Eq. (5) for Δt in terms of Δx and M. Substituting this equation for Δt into 3 gives an expression for λ in terms of fluid material properties and the SRD computational parameters Δx and M. Substituting this into Eq. (7) then gives the Schmidt number as function of $\Delta x/\sigma$.

Figure 1 shows an example of this for our model Lennard-Jones system. In Fig. 1 both $\lambda/\Delta x$ and Δt are plotted as functions of $\Delta x/\sigma$ for various values of M. Note that as M increases $\lambda/\Delta x$ and Δt get smaller or bigger for a given

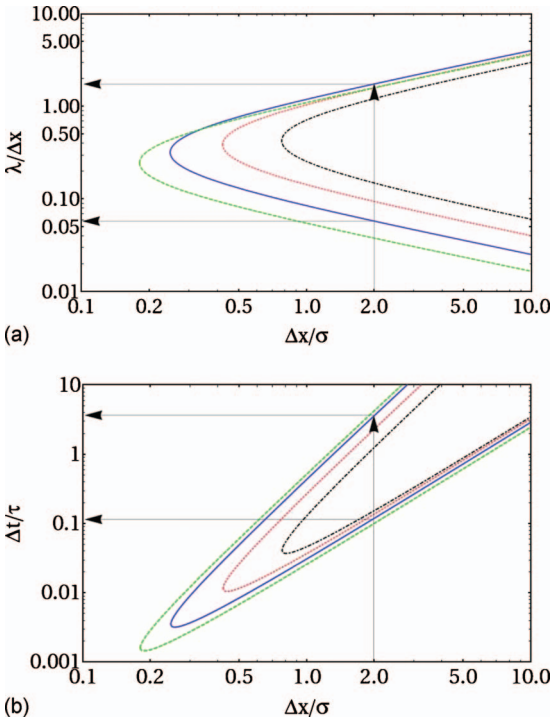

FIG. 1. Possible SRD parameters for modeling a Lennard-Jones fluid with $\nu=1.53\sigma^2/\tau$ and $\rho=0.66m_{\mathrm{LJ}}/\sigma^3$ at $k_BT=\epsilon$ for: $M=3$ (green dashed), $M=5$ (blue solid), $M=10$ (red dotted), and $M=20$ (black dotted-dashed).

$\Delta x/\sigma$ depending on whether one is on upper of lower part of the curve. However, for given $\lambda/\Delta x$ or Δt, $\Delta x/\sigma$ increases with increasing M.

For a given rotation angle α, choosing SRD parameters becomes a matter of specifying Δx, Δt, and M. It should be noted that there are four parameters in this method. M and α clearly have an effect on the value of Sc as can be seen in Fig. 1. Larger values of α lead to larger collisional contribution to the viscosity and thus to larger Sc as explained by Ripoll *et al.*[30] Typically, the choice of M is made so as to be as computationally efficient as possible within any constraints on λ. For the example as shown in Fig. 1, values of $\Delta x=2.0\sigma$ (setting the SRD fluid length scale equal to twice the Lennard-Jones length scale) and $M=5$ for computational efficiency are chosen yielding a λ/σ slightly less than two. These values give $\Delta t\approx3.5\tau$. The reason for choosing the larger of the two possible values for Δt on the $M=5$ curve is that the larger value of λ/σ was selected on the first graph. This serves to make the SRD time step large compared to the explicit atom Lennard-Jones solvent time step δt 0.005τ; reducing the amount of computation at the cost of accuracy in temporal resolution. Selecting the larger time step also leads to a small Sc in Fig. 2. Small Sc can lead to more gaslike than liquidlike behavior; however, increasing the value of the rotation angle as shown in Fig. 2 can increase the value of Sc while keeping all other parameters the same.[30] Finally, m_{SRD} can be determined from the definition of the density given ρ, M, and Δx.

Plotted in Fig. 3 are $\lambda/\Delta x$ and $\Delta t/\tau$ versus $\Delta x/\sigma$ for values of ν and k_BT scaled by 0.5 and 0.25. Notice that as k_BT and ν are scaled to smaller values, the loci of available parameters Δx and Δt shift to longer times and larger lengths

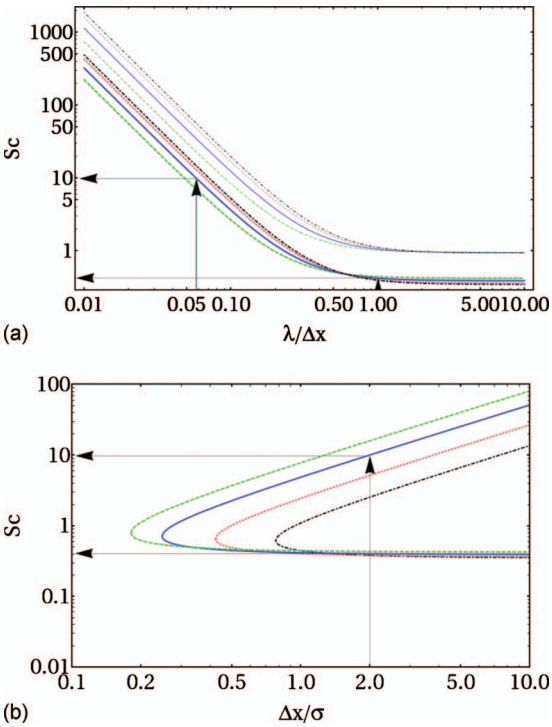

FIG. 2. Values of Schmidt Number for various SRD parameters in modeling a Lennard-Jones fluid with $\nu=1.53\sigma^2/\tau$ and $\rho=0.66m_{\mathrm{LJ}}/\sigma^3$ at $k_BT=\epsilon$ for: $M=3$ (green dashed), $M=5$ (blue solid), $M=10$ (red dotted), and $M=20$ (black dotted-dashed).

for the same $\lambda/\Delta x$. This is useful for simulations involving longer length and time scales using SRD and is an example of "telescoping" or "collapsing" of time scales. For example, if one is interested in simulating a colloidal suspension

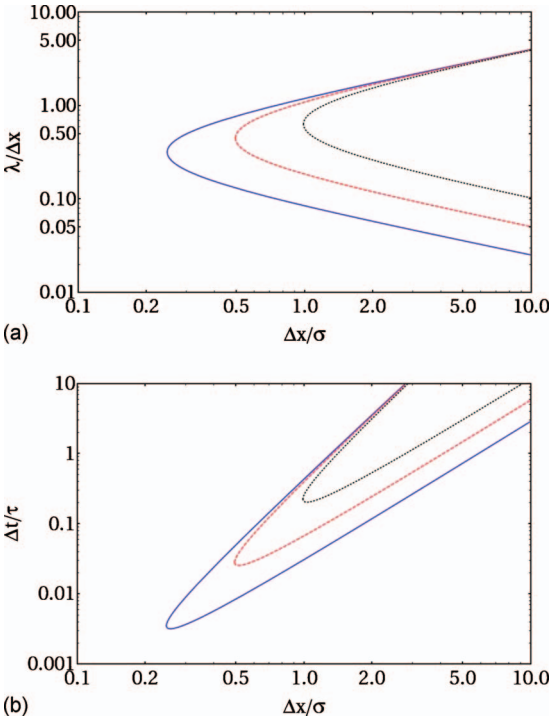

FIG. 3. Possible SRD parameters for $\rho=0.66m_{\mathrm{LJ}}/\sigma^3$, $M=5$ and $\nu=1.53\sigma^2/\tau$, $k_BT=\epsilon$ (blue solid), $\nu=0.765\sigma^2/\tau$, $k_BT=0.5\epsilon$ (red dotted), and $\nu=0.3825\sigma^2/\tau$, $k_BT=0.25\epsilon$ (black dotted-dotted).

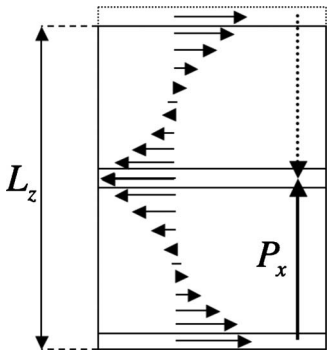

FIG. 4. Velocity profile for MP reverse perturbation method.

where only the equilibrium dynamics of the colloids are of interest, the relevant parameter is the colloid diffusion coefficient D_c. In the dilute limit, according to the Stokes–Einstein relation, $D_c=k_BT/(6\pi\rho\nu R)$. Hence, one can simulate a "dynamically similar" system as far as the dynamics of the colloids is concerned by keeping the ratio of k_BT/ν constant, but reducing the individual values of each by the same factor. Doing so allows access to the longer times and larger length scales noted above. That is, if the colloids are large ($\sim 1000\sigma$) it is helpful to scale the viscosity and temperature while keeping $\lambda/\Delta x$ and thus Sc constant and the mean free path within appropriate bounds (e.g., $\lambda \lesssim a/2$, where a is the radius of the colloid). However, one must keep in mind that changing the kinetic energy scale k_BT requires adjusting the potential energy scale accordingly (e.g., k_BT/ϵ must be constant for an LJ-type system). Whether this is valid for general multiparameter colloid-colloid interaction potentials remains to be determined.

C. Nonequilibrium SRD

In previous simulations shear has been induced either by using Lees–Edwards boundary conditions[24] or by setting the mean velocity **u** in the cells at the border to the shear velocity.[13,14] Here we use the MP (Ref. 26) reverse perturbation method. This method is distinguished from the majority of nonequilibrium molecular dynamics simulations, e.g., the SLLOD algorithm,[34] in that the flux of momentum is induced rather than measured. The momentum is imposed on the system through a series of momentum exchanges between particles within the system. Figure 4 presents a schematic of the simulation box in relation to the important features of the MP algorithm. The simulation box is first divided into n slabs along one coordinate—in this example, the Z coordinate. Two particles are then identified—one in the nth slab and the other in the $((n/2)+1)$th slab—such that their velocities, V_x, are opposed to the desired streaming direction of the corresponding slab. With this particle pair identified, the momentum, p_x, is then exchanged between the two particles. The entire process is repeated at a set interval to produce the desired shear rate. This induced shear rate can be modulated by varying the number of time steps between momentum exchanges, the number of momentum exchanges in a given time step, by exchanging momentum between pairs with velocities less than that of the velocities most opposed to the streaming direction, or any combination of the three.

TABLE I. SRD solvent parameters used in Sec. III such that $T=\epsilon/k_B$, $\nu=1.53\sigma^2/\tau$, and $\rho=0.66m_{\mathrm{LJ}}/\sigma^3$.

Set	$\Delta x[\sigma]$	$\Delta t[\tau]$	M	m_{SRD}	$\lambda/\Delta x$	η	η_c	η_k	Sc	$P[m/\sigma\tau^2]$	$c_s[\sigma/\tau]$
1	2.0	3.5	5.28	1.0	1.75	1.02	0.0340	0.982	0.402	0.66	1.29
2	2.0	2.5	8.8	0.6	1.61	1.00	0.0520	0.952	0.396	1.1	1.67
3	1.0	0.5	3.3	0.2	1.12	1.00	0.0519	0.951	0.515	3.3	2.89
4	2.0	0.9	26.4	0.2	1.01	0.987	0.157	0.830	0.595	3.3	2.89
5	4.0	2.8	70.4	0.6	0.904	1.01	0.207	0.803	0.447	1.1	1.67

As can be seen in Fig. 4, the induced velocity profile is composed of two approximately linear profiles mirrored about the middle of the first and middle slab. This velocity profile, $(\partial v_x/\partial z)$, can be related to the imposed momentum transfer and fluid viscosity,

$$j_z(p_x) = -\eta\frac{\partial v_x}{\partial z}. \tag{8}$$

The amount of momentum exchanged at each time step is known exactly, and the total momentum transfer, P_x, is tabulated over the course of the shearing trajectory. From the total momentum transfer, the momentum flux can be calculated,

$$j_z(p_x) = \frac{P_x}{2tA}, \tag{9}$$

where $A=L_xL_y$, the cross sectional area, t is the length of the trajectory, and the factor of 2 accounts for the periodicity of the restoring momentum flow.

Since the MP algorithm conserves both total momentum and total energy and SRD is an *NVE*-type method, no thermostat is required. However, at high shear rates the system may need to be initialized at a higher thermal energy since upon shearing, the random kinetic (thermal) energy will be converted into the streaming kinetic energy of the average flow field. The absence of a thermostat simplifies matters greatly. One of the more compelling advantage being that the shear profile of the system is a response to the momentum transfer rather than being a function of the thermostat.

III. RESULTS

All results discussed below have in view a typical low viscosity fluid as the solvent for which SRD is to provide a model for the multibody, long-range, unsteady, fluctuating hydrodynamic interactions between colloids. In particular, as noted above, the solvent is modeled as a system of Lennard-Jones particles at $k_BT=\epsilon$. For $r_c=3.0\sigma$, the resulting kinetic viscosity and density are $\nu=1.53\sigma^2/\tau$ and $\rho=0.66m_{\mathrm{LJ}}/\sigma^3$ respectively.

Several values of the SRD fluid parameters were chosen as shown in Table I, each consistent with an LJ solvent described above. The majority of results in the following are for the first row of parameters for which the number density of the LJ and SRD fluids are equivalent. Also shown in the last two columns are the value of the pressure from the ideal gas equation of state and the value of the speed of sound c_s for the SRD parameters listed. Note that from the SRD equation of state the pressure in the SRD fluid can be large relative to the explicit atom LJ solvent nominal pressure ($\sim 0.1m/\sigma\tau^2$) in comparable simulations.[35]

Assuming that the mass density of the SRD fluid equal that of the LJ system gives $\Delta x=(Mm_{\mathrm{SRD}}/\rho_{\mathrm{LJ}})^{1/3}$. This serves to illustrate the freedom one has in choosing SRD fluid parameters that are consistent with the desired LJ material parameters. For $m_{\mathrm{SRD}}=m_{\mathrm{LJ}}=\sigma=1.0$ and $\rho_{\mathrm{LJ}}=0.66$, any $\Delta x=(M/0.66)^{1/3}$ is possible suggesting that there is no "natural" length scale in an SRD fluid such as the size of a constituent LJ atom. However, for colloidal suspensions, the radius a of the colloid introduces a nature length scale such that $\Delta x<a$. Values of M used in the following are shown in Table I. The majority of results are for $M=5.28$ and $\Delta x=2.0$. Given these, Δt can be found and satisfaction of constraints on Sc can be verified if required (cf. Fig. 1). Note that for the present case of comparing to an LJ solvent no scaling of the viscosity or temperature is required since all the SRD parameters are within reasonable ranges. This is due to the relatively small size of the SRD bins, e.g., $\Delta x\sim\sigma$. In general, exactly matching solvent properties can be computationally expensive especially when larger length and time scales are required such as for simulating large colloidal particles.[11]

In the present case of one-to-one matching between a LJ-type solvent and an SRD fluid, the key physical values of the LJ-fluid can be met without "telescoping" the time scales. That is, we simulate the exact density, kinematic viscosity, and temperature of the LJ-fluid without approximation. To this point we are modeling the correct form of the Navier–Stokes equations (i.e., fluctuation, nonsteady, low Reynolds number, Newtonian flow). If the exact number density and system size are simulated, the SRD simulations contain the same number of SRD particles as an LJ solvent contains LJ atoms. To obtain the same mass density for the SRD and LJ systems, we simply set the mass of the SRD particle to be the same as a LJ atom. Since the SRD particles have an ideal gas equation of state, the speed of sound in the fluid $(c_s=\sqrt{(5/3)(k_BT/\rho_f)(M/\Delta x^3)})$ and the Mach number of the SRD system $(\mathrm{Ma}=v_s/c_f)$ are not that of the LJ solvent system. This is an indication that the SRD fluid cannot capture the "correct" thermodynamics of the solvent and means that the SRD fluid always has an artificially high compressibility compared to the LJ fluid. However, again due to the small length and time scales considered here, the values of the speed of sound in the SRD fluid are reasonable compared to LJ solvent values,[36] which means there is no flow velocity limitation in order to keep the Mach number low. It should also be noted that because SRD particles are ideal the pure SRD fluid has zero bulk viscosity. So that if the LJ fluid is

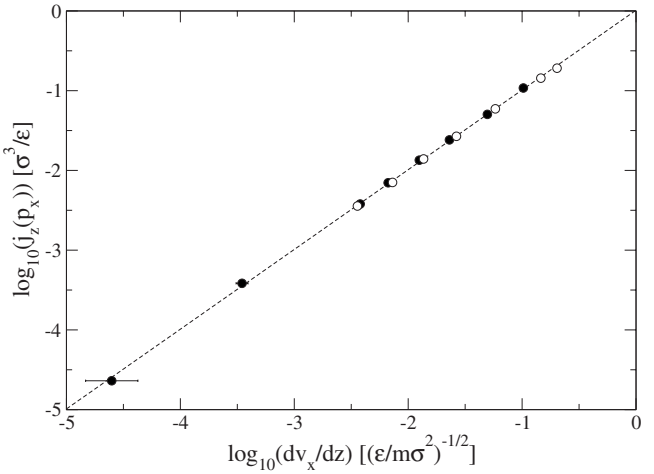

FIG. 5. Linear response relation between the shear rate and momentum flux for a Lennard-Jones fluid (open symbols) and SRD fluid with parameter set 1 (closed symbols).

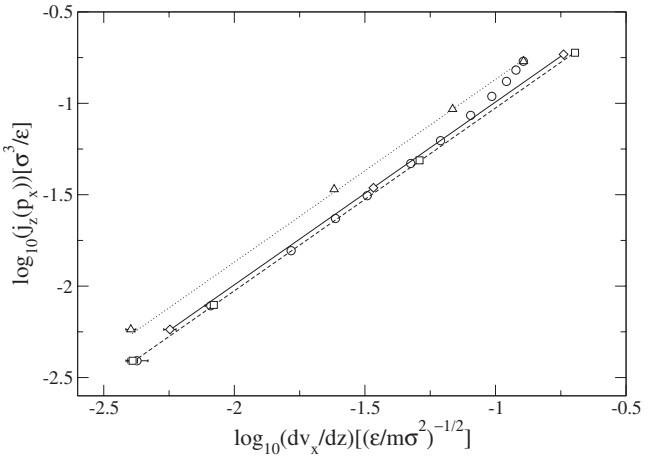

FIG. 6. Effect of the momentum exchange rate and particle velocity on the momentum transfer and resulting viscosity—multiple exchanges per time step of low velocity particles (square, dashed line), varied exchange frequencies of high velocity particles (triangle, dotted line), single exchange per time step of increasing velocity particles (circle), and varied exchange frequencies of high velocity particles using the smaller SRD time step (diamonds, solid line).

incompressible, the only error introduced due to artificial compressibility in the SRD fluid is from the shear viscosity term in the Newtonian viscous stress tensor.[17]

Additionally, the Schmidt number in Eq. (7), which is a measure of diffusive momentum transfer relative to the diffusive mass transfer in the fluid, and the Knudsen number ($\mathrm{Kn}=\lambda_f/\Delta x$, where Δx defines the relevant length scale of the fluid), which characterizes noncontinuum effects, may be different between the SRD and LJ fluids. While the Schmidt number does not effect the Navier–Stokes equations as noted for colloidal suspensions,[9] it has been found to have significant effect on the dynamics of SRD particles in pure fluid systems.[30] We will discuss this in more detail below, but it is sufficient to note at this point that $\mathrm{Sc}\sim 10$ in an LJ fluid.[33] For comparable mean free paths in SRD and LJ fluids, the Knudsen number would also be equivalent in the two simulations; however, this is not expected to be the case here. In fact, the Knudsen number for the SRD simulations is about an order of magnitude larger than the LJ solvent. In the current simulations these are potentially the largest sources of error due to the coarse graining of the LJ solvent.

Using the MP approach described in Sec. II, the shear viscosity of the pure SRD fluid was measured for several parameter sets (see table I). Within the regime of linear response a log-log plot of the induced shear rate and the imposed momentum transfer will fall on a line of slope 1. The viscosity in the limit of zero shear can then be calculated from the y-intercept of the best fit line through the points within this linear response regime. Figure 5 compares such a plot for a Lennard-Jones system at the above described state point and SRD parameter set 1. Notice that with the SRD, quite low shear rates are possible. The Lennard-Jones system exhibited shear thinning for the highest shear rates. Newtonian behavior was observed at all shear rates simulated in the SRD systems.

The manner in which the MP momentum transfer is performed must account for the nonuniform kinetic and collisional contributions to the momentum flux within an SRD bin.[24] One way to accommodate the nonuniform contributions is to make the MP bins the same size as the SRD bins. The particles chosen for the momentum exchange will then have an equal likelihood of being chosen from any point within the SRD bin. Alternately, SRD bin shifting can be used to effectively randomize the location of the chosen particle in relation to the SRD bin. Both methods were found to yield equivalent results. In either case, the bins containing particles participating in the momentum exchanges were discarded in the analysis of the velocity profile.

As mentioned in Sec. II, the momentum transfer can be modulated by varying the frequency that the momentum exchanges are performed, as well as choosing particles with velocities of different magnitudes relative to the desired streaming direction and velocity. If the SRD time step is used as the integration time step, that is, the particles are advected and rotated in a single operation, then the momentum exchange can only be performed a single time per collision/streaming step. However, if the integration time step was smaller than the SRD collision time step (say 0.1, a time step appropriate for a 20σ sized colloidal particle), then significant flexibility is gained in choosing momentum exchange frequencies tailored to drive a desired shear rate. Using a common time step between the various parameter sets has the additional benefit of removing the disparate SRD time steps as a factor in the imposed momentum transfer.

It was found that the velocity of the particles chosen for the MP momentum exchange had a dramatic effect on the momentum flux, and the resulting measured viscosity. Three series of simulations were run to investigate this effect. Figure 6 contains the data for these three series, all using the parameters of set 4 in Table I, an integration time step $\Delta t=0.1$, with a system volume of $8^3\sigma^3$. The circles in Fig. 6 represent a series simulations where the momentum exchange was performed every time step between particle pairs with successively smaller velocities, resulting in smaller imposed momentum transfer and induced shear rate. As the magnitude of the velocity exchanged between two particles is increased, the points eventually deviate from the apparent

linear relationship exhibited by the points representing smaller values of velocity exchanges. In order to identify if this deviation at high shear rates is due to the magnitude of the velocities exchanged or just the imposed momentum transfer, two additional series of simulations were performed. The second series (Fig. 6, triangles) exchanged particle velocities which were the most opposed velocities relative to the streaming direction, but performed the exchange at successively lower frequency, generating lower imposed momentum transfer and concomitant shear rates. The third series (Fig. 6, squares) exchanged velocities between particle pairs such that the velocities were within the linear regime of the first series of simulations, but for a successively larger number of particles within a given time step.

For large values of momentum exchange between high velocity particles, the imposed momentum transfer deviates from the momentum flux and the resulting shear rate. This can be seen by comparing the series 1 curve (Fig. 6, circles), to the series 2 curve (Fig. 6, triangles). For a common value of imposed momentum transfer the resulting shear rate is smaller for the series where pairs with the largest velocities were chosen for the momentum exchange (series 2), indicating a lower momentum flux. Likewise, comparing the series 3 curve (Fig. 6, squares) to the high velocity points of the series 1 curve, a higher shear rate is exhibited for the series 3 curve (multiple exchanges of small velocities in a single time step) for equivalent imposed momentum transfer. Apparently, exchanges between high velocity particles, not large momentum transfer, result in an anomalously low momentum flux. For each point that deviates from the linear region—that is, points generated by performing momentum exchanges between particles with some chosen large velocity—there is a curve that can be created through successively less frequent momentum exchanges between particles with that chosen large velocity value. This curve will be linear in imposed momentum transfer and induced shear rate. In order to avoid calculating a spurious viscosity resulting from exchanges between particles with too-large velocities, a curve is generated using exchanges between particles with successively smaller velocities (as in Fig. 6, circles). From this curve an appropriately small velocity value is chosen from the linear region and a new curve is generated by modulating the imposed momentum transfer through multiple exchanges in a single time step between multiple particle pairs with the chosen velocity (as in Fig. 6, squares). The viscosity is then taken from the y-intercept of the best-fit line of slope 1 passing through the points.

The viscosity of the SRD systems also exhibits finite size effects as shown in (Fig. 7). Each set of parameters from Table I were simulated at a fixed density but with progressively larger system size. In general, all systems manifest viscosities lower than expected from Eq. (5) for the smallest systems simulated. Two sets (set 4 and set 5) converged to the expected viscosity at relatively small system sizes. These parameters are distinguished by the comparatively larger contribution of the collisional component of the viscosity (see Table I). As discussed in Sec. II, for a fixed set of SRD parameters the larger of two possible time steps was chosen for computational efficiency. If the smaller is used, then the

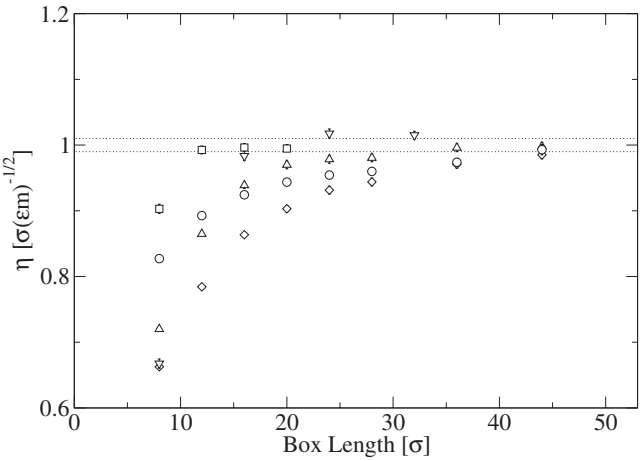

FIG. 7. Effect of a finite sized simulation box on the shear viscosity for various parameters: set 1 (diamonds), set 2 (triangle), set 3 (circle), set 4 (square), and set 5 (inverted triangle). The viscosity values of the various sets are bounded by the dotted lines.

collisional contribution dominates the kinetic contribution to the viscosity. The diamonds in Fig. 6 are for points calculated using the smaller of the two possible time steps for the same system size and the otherwise identical SRD parameters of set 4. While the viscosity calculated from the simulation set wherein the momentum exchange was between particles with the most opposed velocities (Fig. 6, triangles) overestimated the expected viscosity by 37%, the set created using the smaller time step found the viscosity to be within 3% of the expected viscosity—with the velocity of the exchange particle having no discernible effect on the induced shear rate. The smaller time step uniformly eliminated the finite size effects for all parameter sets considered. It has been shown[30] that long time velocity correlations of an SRD fluid exhibit anomalously fast decay. This was explained by analogy to similar systems where the hydrodynamic modes were truncated by the system size. The truncation of the hydrodynamic modes is apparently a more severe restriction for the more gaslike simulation, that is, the simulations using the larger of the two possible time steps. While the anomalous viscosity is possibly related to the MP method, it seems unlikely given the convergence of the viscosity for a particular sized system with decreasing velocity of the exchange pair. The smallest of these velocities being a very small perturbation to the fluid relative to the average particle velocity.

Small values of the collision time step significantly reduce the efficiency of the simulation. Depending on the ratio of the kinetic to collisional contribution to the total viscosity for a given set of parameters, using the larger time step might be sufficient to model the desired viscosity for a modestly sized system. Alternately, if a large system size is otherwise necessary because of the number or size of embedded particles, the larger time step may be adequate given that the system is large enough to capture the relevant hydrodynamic modes.

IV. IMPLEMENTATION

In this section we discuss the implementation of SRD in our parallel molecular dynamics (MD) code LAMMPS (Ref.

37) and present some performance results. Like many MD codes, LAMMPS achieves improved parallel performance by partitioning the overall simulation box into small brick-shaped subdomains, one per processor.

A time step in MD consists of computing forces between particles (usually via a neighbor list that stores pairs of nearby particles), performing time integration to update the positions and velocities of particles using these forces, and calculating other diagnostic or output quantities. In parallel, each processor does this for the particles in its subdomain, with some communication required to acquire nearby "ghost" particles owned by neighboring processors.

SRD differs from usual MD in that SRD particles do not interact with each other in a pairwise sense, thus neighbor lists need not include them, nor are forces on SRD particles computed. When a mixture simulation is performed (e.g., large colloidal particles in a background SRD fluid), then collisions between SRD and colloidal particles do impart force to the SRD particles, which introduces some additional issues. In this paper we are only concerned with the SRD advection and rotation operations and how to perform them efficiently in parallel. We do this in LAMMPS by partitioning the overall set of particles on each processor into two groups, SRD and non-SRD particles. Since particle attributes are stored in lists (vectors), this simply means the non-SRD particles are at the beginning of the list, and SRD particles at the end. This is maintained as particles move from one processor's geometric domain to another during the simulation and processors add/delete particles to/from their lists. The advantage of this approach is that all the normal MD operations (neighbor list construction, pairwise force computation, time integration) can easily exclude SRD particles, by only looping over the first portion of the list. Likewise, ghost versions of SRD particles, owned by nearby processors, are not needed in our implementation of the SRD algorithm and hence are not communicated; only non-SRD particles are ghosted. We note that these savings are critical in a performance sense, because the ratio of SRD to non-SRD particles can easily be 1000 to 1 or greater. In a pure SRD simulation, no non-SRD particles exist; these operations are effectively not even invoked.

LAMMPS allows new features to be added by writing a "fix" (a C++ class) which includes methods (subroutines) that are invoked at different stages of the MD time step. The SRD model was implemented in this manner, as a single new class. One method advects the SRD particles each time step. A second method performs the rotation operation to collectively change the velocities of SRD particles in the same SRD bin. We discuss each in turn.

The advection operation is trivial: $x_{\mathrm{new}}=x_{\mathrm{old}}+v\Delta t_c$ for each SRD particle, where x and v are its position and velocity; the velocity does not change since there are no forces. The time step Δt_c requires some discussion. In a mixture simulation there are two time scales: $\Delta t_c<\Delta t_s$. The shorter colloid time scale is used to compute colloid-colloid interactions and advect the colloid particles. Note that even though Δt_c is small in the SRD context, it is a function of the mass and interaction strength of the large colloidal particles, and is thus much larger than the time step that would be required to integrate solvent-solvent interactions in, for example, a Lennard-Jones (LJ) background fluid. Δt_s is the time scale on which SRD particle velocities are rotated.

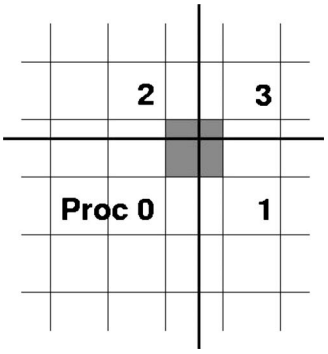

FIG. 8. Portion of a 2d simulation box, owned by processor 0, 1, 2, and 3. The heavy lines represent processor boundaries; the light lines are the grid of SRD bins. The shaded bin overlaps the subdomains owned by all four processors.

In a pure SRD simulation, these two time scales could be collapsed into a single large time step. Each Δt_s, SRD particles would advect for a full step and then be binned and their velocities rotated. However, we choose here to maintain a separation of the two time scales, advecting SRD particles once every Δt_c, and rotating their velocities once every Δt_s. This is to match what we do in a mixture and because taking very large SRD advection steps can cause problems in a mixture, e.g. if a SRD particle moves far inside or even passes through a colloid particle, complicating collision detection and resolution. In the benchmark discussed below, $\Delta t_s=3.5$ (chosen to map the SRD fluid to a LJ fluid) and $\Delta t_c=0.1$ (a typical time step for colloids or nanoparticles of size 20σ). Thus SRD particles advect for a full SRD time step in 35 shorter Δt_c increments.

In parallel, SRD particles can move outside a processor's subdomain as they advect. This is allowed in LAMMPS; particles are not moved to new processors until a reneighboring is performed. In a mixture simulation, reneighboring would be triggered by colloid movement and typically occurs every few Δt_c steps. In a pure SRD simulation it is triggered by the SRD rotations, i.e., every 35 steps in this benchmark.

We require SRD particles to be inside the subdomain of the processor that owns them when the rotation operation is done, carried out by superimposing a set of SRD bins as a three dimensional (3d) grid across the entire simulation domain. For a periodic system we require there to be an integer number of bins in each dimension. As discussed in Sec. II, if the mean-free path λ of SRD particles is less than 0.6 of the bin size s, then the alignment of the grid relative to the simulation box is shifted randomly in each dimension by an offset of up to s in magnitude. This is done each time a rotation operation is performed, to avoid undesirable correlations in the rotated velocities. This means some bins will overlap the subdomains of multiple processors, as in Fig. 8 for a two dimensional (2d) example where the shaded bin overlaps in both x and y. Even if bin shifting is not required ($\lambda>0.6s$), overlaps will still occur if the number of bins in any dimension is not a multiple of the number of processors in the corresponding dimension. Note that Fig. 8 could also repre-

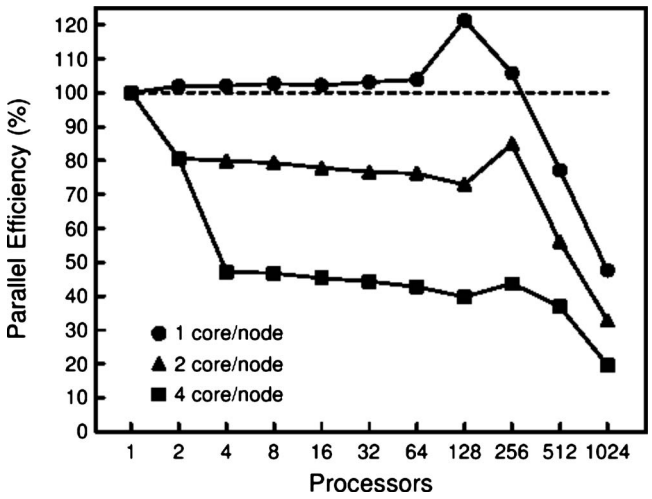

FIG. 9. Parallel efficiency of an SRD simulation of 4.7×10^6 particles running on different numbers of processors (cores) of a Cray XT3. The three curves are for running 1, 2, and 4 cores/node. The one-core timing was 207 s for 1050 time steps.

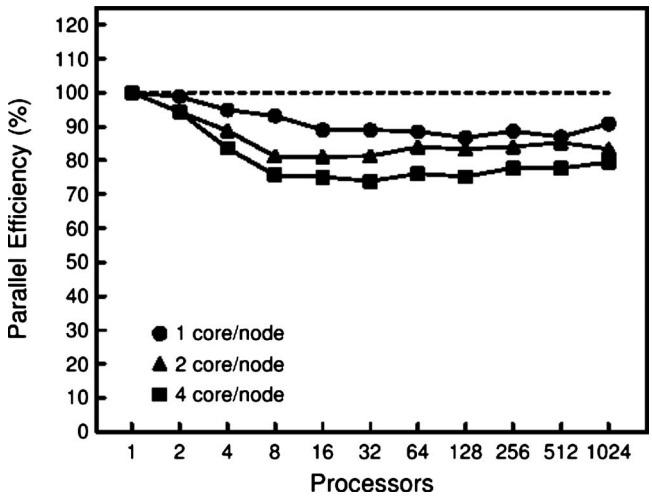

FIG. 10. Parallel efficiency of an explicit LJ simulation of 4.7×10^6 particles running on a Cray XT3, analogous to the SRD model of Fig. 9. The one-processor timing was 9567 seconds for 1050 time steps.

sent the overlap that occurs at a periodic boundary due to bin shifting. If the dark vertical line was a periodic boundary, then processors 0 and 1 would own subdomains at opposite x ends of the simulation box.

To compute new velocities, each processor first loops over its SRD particles, determines which bin each is inside, and sums each particle's velocity vector to the total velocity for that bin. For overlapping bins, the partial velocity sum and count of contributing particles are then communicated to the other processors that share the bin. This is done efficiently by precomputing the list of bins that overlap in each dimension, namely, those on the six faces of a processor's subdomain. Messages are first exchanged (send and receive) in the x direction, then in y, finally in z, with the six neighbors of each processor. A bin with overlaps in more than one dimension, such as the shaded bin in Fig. 8, is sent multiple times. When this operation is complete, each processor knows the total summed velocity and particle count for all bins it either owns entirely or overlaps with. Thus it can compute the average particle velocity in those bins and perform the rotation operation to adjust the velocity of all SRD particles it owns. The latter involves choosing a random axis to rotate around for each bin. Processors sharing a bin do this consistently by having the lowest-index processor (processor 0 for the shaded bin in Fig. 8), compute a random number which is included in the data exchanged for that bin. Note that the total amount of data communicated in this operation is proportional to the number of overlapping bins, not to the number of SRD particles. Hence it is a relatively cheap operation, especially if there are many SRD particles per bin.

Figure 9 shows the parallel performance of our SRD implementation for a pure SRD simulation with 4.7×10^6 particles and a 96^3 SRD grid, one of the models discussed in Sec. III. The two time steps used were $\Delta t_c=0.1$ (for advection) and $\Delta t_s=3.5$ (for rotation), in reduced LJ units. Randomized bin shifting was used in the rotation operation. The runs were performed on a Cray XT3 with quad-core 2.2 GHz AMD Opteron nodes and a custom interconnect. Timing curves are shown for running in three different modes, using 1, 2, or all 4 cores per node. For example, running on 512 processors (cores) with 2 cores/node, means 256 Opteron nodes were used (and only half the available cores).

The single-core timing for this SRD problem, assumed to be 100% efficient, was 206.9 seconds for a 1050 Δt_c time step run (advecting every step, rotating every 35 steps). The time to perform a rotation operation was about nine times more than an advection time step. A parallel efficiency of 80% on 512 processors of the 1 core/node curve means the simulation ran about 400 times faster than it did on one core, i.e. in 0.54 s in this case. The vertical offsets between the three curves are due to limited memory bandwidth on an Opteron node when using multiple cores. Once this cost has been paid (running on two or four processors for the two core and four core curves), then performance scales nicely out to about 256 processors. The small bump in performance in all three curves near this processor count is likely due to particle lists fitting into cache once the particle count per processor is small enough. Past this point, communication or other overhead costs begin to dominate and the performance degrades for all three curves.

The performance degradation when there are a few thousand SRD particles per processor is partly because the simulation is running so fast (thousands of time steps per CPU second). For comparison, Fig. 10 shows parallel efficiency curves for an explicit LJ solvent simulation with the same number and density of particles ($N=4.7\times10^6$, $\rho^*=0.66$, $T^*=1.0$, cutoff$=2.5\sigma$). Neighbor lists were now employed to find pair interactions efficiently; the lists were rebuilt on average every 6 time steps. The additional computation required to calculate solvent-solvent interactions has two effects. There is enough computation that multiple cores per Opteron can be used more effectively without saturating memory bandwidth. And there is no performance degradation even at 1024 processors when there are fewer than 5000 particles per processor.

However, the explicit LJ model required 9567 s to run for 1050 time steps on a single core, which is 46 times

slower than the SRD model. Additionally, the SRD time step of 0.1 (in reduced units) is 20 times larger than the standard LJ time step of 0.005. Since these are multiplicative factors, this means that when the SRD model is applicable, it can enable much larger and faster simulations of pure or mixture systems than would be possible with explicit LJ solvent.

V. CONCLUSION

The implementation of SRD for simulating mesoscale hydrodynamics has been discussed. As a means for modeling fluctuating hydrodynamics in colloidal suspensions, SRD is more computationally efficient than simulations containing atomistic (LJ) solvents. Additionally, it has been shown that in certain approximations which "collapse" or "telescope" time scales are not necessary. Here the SRD fluid was parametrized to model an LJ-type solvent at a given temperature and density with a known shear viscosity.

We demonstrated the novel combination of the SRD fluid model with the MP reverse perturbation method for measuring shear viscosity. The SRD model presented several unique considerations when used in conjunction with the MP method. Due to the nonuniform momentum flux of the kinetic and collisional components, individual MP swap bins must either be aligned with a plane of full SRD bins, or SRD bin shifting must be implemented. Additionally, depending on the potential for finite size effects, the value of the velocity of the particles swapped in the MP method must be taken into account. For small systems with a modest collisional contribution to the viscosity the velocity of swapped particles should be chosen to achieve the correct restoring momentum flux for the imposed momentum transfer.

ACKNOWLEDGMENTS

This work was performed, in part, at the Center for Integrated Nanotechnologies, a U.S. Department of Energy, Office of Basic Energy Sciences user facility. Funding for this work was provided through the National Institute for Nano-Engineering and by the Laboratory Directed Research and Development program at Sandia National Laboratories. Sandia National Laboratories is a multiprogram laboratory operated by Sandia Corporation, a Lockheed-Martin Company, for the U.S. Department of Energy under Contract No. DE-AC04-94AL85000.

[1] D. R. Foss and J. F. Brady, J. Fluid Mech. **407**, 167 (2000).
[2] A. J. C. Ladd and R. Verberg, J. Stat. Phys. **104**, 1191 (2001).
[3] P. Español, Phys. Rev. E **57**, 2930 (1998).
[4] A. Malevanets and R. Kapral, J. Chem. Phys. **110**, 8605 (1999).
[5] A. Malevanets and R. Kapral, J. Chem. Phys. **112**, 7260 (2000).
[6] Y. Inoue, Y. Chen, and H. Ohashi, J. Stat. Phys. **107**, 85 (2002).
[7] S. H. Lee and R. Kapral, J. Chem. Phys. **121**, 11163 (2004).
[8] J. T. Padding and A. A. Louis, Phys. Rev. Lett. **93**, 220601 (2004).
[9] J. T. Padding and A. A. Louis, Phys. Rev. E **74**, 031402 (2006).
[10] J. T. Padding and A. A. Louis, Phys. Rev. E **77**, 011402 (2008).
[11] M. Hecht, J. Harting, T. Ihle, and H. J. Herrmann, Phys. Rev. E **72**, 011408 (2005).
[12] A. Wysocki, C. P. Royall, R. G. Winkler, G. Gompper, H. Tanaka, A. van Blaaderen, and H. Löwen, Faraday Discuss. **144**, 245 (2010).
[13] M. Hecht, J. Harting, M. Bier, J. Reinshagen, and H. J. Herrmann, Phys. Rev. E **74**, 021403 (2006).
[14] M. Hecht, J. Harting, and H. J. Herrmann, Phys. Rev. E **75**, 051404 (2007).
[15] M. Ripoll, P. Holmquist, R. G. Winkler, G. Gompper, J. K. G. Dhont, and M. P. Lettinga, Phys. Rev. Lett. **101**, 168302 (2008).
[16] M. Ripoll, R. G. Winkler, K. Mussawisade, and G. Gompper, J. Phys.: Condens. Matter **20**, 404209 (2008).
[17] G. Gompper, T. Ihle, D. M. Kroll, and R. G. Winkler, Adv. Polym. Sci. **221**, 1 (2009).
[18] R. Kapral, Adv. Chem. Phys. **140**, 89 (2008).
[19] T. Ihle and D. M. Kroll, Phys. Rev. E **67**, 066705 (2003).
[20] T. Ihle and D. M. Kroll, Phys. Rev. E **67**, 066706 (2003).
[21] E. Tüzel, M. Strauss, T. Ihle, and D. M. Kroll, Phys. Rev. E **68**, 036701 (2003).
[22] T. Ihle and D. M. Kroll, Phys. Rev. E **70**, 035701R (2004).
[23] T. Ihle, E. Tüzel, and D. M. Kroll, Phys. Rev. E **72**, 046707 (2005).
[24] N. Kikuchi, C. M. Pooley, J. F. Ryder, and J. M. Yeomans, J. Chem. Phys. **119**, 6388 (2003).
[25] C. M. Pooley and J. M. Yeomans, J. Phys. Chem. B **109**, 6505 (2005).
[26] F. Müller-Plathe, Phys. Rev. E **59**, 4894 (1999).
[27] H. Guo, K. Kremer, and T. Soddemann, Phys. Rev. E **66**, 061503 (2002).
[28] P. J. in 't Veld, M. K. Petersen, and G. S. Grest, Phys. Rev. E **79**, 021401 (2009).
[29] W. Zhao, F. Leroy, S. Balasubramanian, and F. Müller-Plathe, J. Phy. Chem. B **112**, 8129 (2008).
[30] M. Ripoll, K. Mussawisade, R. G. Winkler, and G. Gompper, Phys. Rev. E **72**, 016701 (2005).
[31] T. Ihle and D. M. Kroll, Phys. Rev. E **63**, 020201 (2001).
[32] E. Tüzel, T. Ihle, and D. M. Kroll, Phys. Rev. E **74**, 056702 (2006).
[33] K. Meier, A. Laesecke, and S. Kabelac, J. Chem. Phys. **121**, 9526 (2004).
[34] M. E. Tuckerman, C. J. Mundy, S. Balasubramanian, and M. L. Klein, J. Chem. Phys. **106**, 5615 (1997); D. J. Evans and G. P. Morriss, *Statistical Mechanics of Nonequilibrium Liquids* (Academic, New York, 1990).
[35] P. J. in 't Veld, S. J. Plimpton, and G. S. Grest, Comput. Phys. Commun. **179**, 320 (2008).
[36] K. Meier and S. Kabelac, J. Chem. Phys. **124**, 064104 (2006).
[37] S. Plimpton, J. Comput. Phys. **117**, 1 (1995).